Biosensors and Bioelectronics xxx (xxxx) xxx

Contents lists available at ScienceDirect

Biosensors and Bioelectronics

journal homepage: http://www.elsevier.com/locate/bios

Coreactant-free electrochemiluminescence biosensor for the determination of organophosphorus pesticides

Ying He [a], Jiawei Du [b], Jinhua Luo [a], Shihong Chen [a,*], Ruo Yuan [a]

[a] Key Laboratory of Luminescence and Real-Time Analytical Chemistry (Southwest University), Ministry of Education, College of Chemistry and Chemical Engineering, Southwest University, Chongqing, 400715, PR China
[b] Chongqing No.8 Secondary School, Chongqing, 401120, PR China

ARTICLE INFO

Keywords:
PFBT PNPs
H_2O_2
Organophosphorus
Enzyme
Biosensor

ABSTRACT

Poly [(9,9-dioctylfluorenyl-2,7-diyl)-co-(1,4-benzo-{2,1',3}-thiadazole)] (PFBT) was functionalized with carboxyl groups *via* nanoprecipitation method to prepare polymer nanoparticles (PNPs). Remarkable electrochemiluminescence (ECL) was observed at PFBT PNPs without any external species or dissolved O_2 as coreactants. Furthermore, such an ECL emission could be efficiently quenched by hydrogen peroxide (H_2O_2). A coreactant-free ECL enzyme-based biosensor is making use of PFBT PNPs as luminophore for detecting organophosphorus (OPs) pesticides. In the absence of OPs, H_2O_2 stemmed from the enzymatic reaction would quench the ECL signal of PFBT PNPs, resulting in an ECL signal-off state. In the presence of OPs, the ECL signal obviously increased because the enzyme activity of the acetylcholinesterase (AChE) was inhibited by OPs. The linear range for OPs detection was 1.0×10^{-12}–1.0×10^{-7} M and the detection limit was low as 1.5×10^{-13} M. Such a coreactant-free ECL strategy could avoid the drawbacks resulted from the addition of exogenous species or dissolved O_2 as coreactant. More importantly, H_2O_2 was released by many oxidases-induced reactions, and its quenching effect on the ECL of PFBT PNPs would pave a new avenue for constructing coreactant-free enzyme-based ECL biosensor for environmental monitoring and biological analysis.

1. Introduction

Electrochemiluminesence (ECL), as a new class of techniques, had attracted widely attention in biological analysis, environmental monitoring, and clinical diagnosis owing to the fast respond, high sensitivity, and low-cost as well as easy controllability (Chinnadayyala et al., 2019). In ECL detection, a highly sensitive detection of the target not only depended on the high luminous efficiency of the luminophore, but also depended on the effective signal switching mode.

In order to achieve a high ECL efficiency of the luminophore, the coreactants of the luminophores were commonly needed. Common strategies for applying the coreactants had their own shortcomings. For example, directly adding coreactants to the detection solution would change the microenvironment of the test system and result in a poor reproducibility and stability of the ECL detection (Jiang et al., 2019; Wang et al., 2009). Immobilizing coreactants on the electrode surface might involve a complicated pretreatment process. Perhaps, the coreactants were easily leaked from the electrode surface in this case (Muzyka et al., 2017). Applying dissolved oxygen (O_2) as coreactant would also encounter a poor repeatability and stability problems due to the uncertainty of its concentration since it was lightly susceptible to temperature and pressure (Kitte et al., 2017; Wang et al., 2012). Furthermore, most of coreactants were environmentally harmful and were inappropriate for the detection in a specific test solution such as cytosol. Therefore, it was very valuable to develop an ECL system excluding exogenous species or dissolved O_2 as coreactant.

In addition to the application of coreactants, seeking an excellent ECL luminophore was also crucial branch to ensure a high ECL efficiency. Various ECL luminophors such as luminol (Wang et al., 2019), ruthenium (II) tris (2, 2′-bipyridyl) ($Ru(bpy)_3^{2+}$) (Qin et al., 2018), quantum dots (Stewart et al., 2018), graphene carbon nitride (g-C_3N_4) (Sha et al., 2019) and metal nanoclusters (Zhou et al., 2018b) had been utilized for bioanalysis. However, these systems generally required exogenous species or dissolved O_2 as coreactants to obtain satisfactory results. Compared with these traditional luminophores, the polyfluorene performed a superior photon-brightness and photostability, and was well applied to cellular sensor or imaging *in vivo* or *in vitro* (Wu and Chui, 2013; Wu et al., 2008). For example, poly (9,9-dioctylfluorenyl-2,7-diyl)

* Corresponding author.
E-mail address: cshong@swu.edu.cn (S. Chen).

https://doi.org/10.1016/j.bios.2019.111898
Received 16 September 2019; Received in revised form 24 October 2019; Accepted 14 November 2019
Available online 18 November 2019
0956-5663/

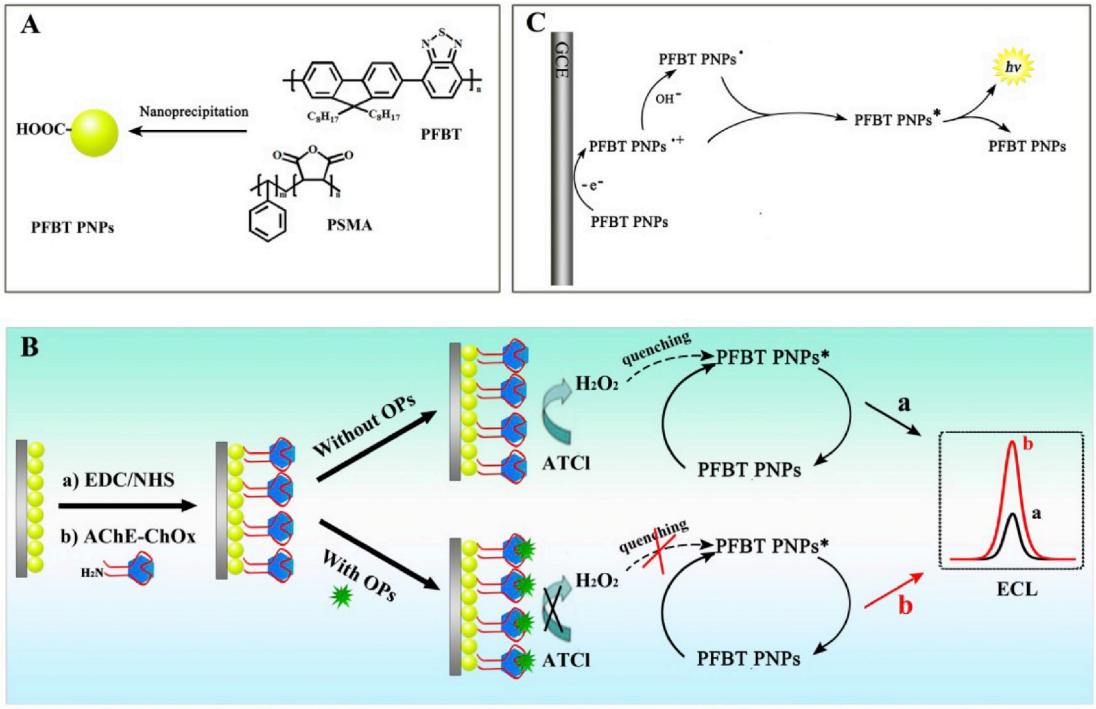

Scheme 1. The preparation of PFBT PNPs (A); the construction of enzyme-based biosensor and quenching effect of H_2O_2 on the ECL of PFBT PNPs (B); the possible ECL emission of PFBT-PNPs (C).

(PFO) dots were reported as an ECL luminophore for H_2O_2 and choline detection (Chen et al., 2016). Ju's group designed an ECL imaging sensor for Fe^{3+} detection using poly [2-methoxy-5-(2-ethylhexyloxy)-1, 4-(1-cyanovinylene-1, 4-phenylene)] (CN-PPV) Pdots as luminophore (Feng et al., 2018). In these reported ECL systems based on polyfluorene, the coreactants such as $C_2O_4^{2-}$ or triethylamine were usually used to enhance the ECL signal. Although PFO dots had been reported as an ECL emitter to achieve the Cu^{2+} detection without any external coreactants in our previous work (Luo et al., 2018), thus opening up a new application prospects of polyfluorene dots in coreactant-free ECL sensing technologies, the ECL luminous efficiency and the stability of PFO dots system need to be further improved.

The ECL signal switching modes were generally divided into two cases, namely, "signal on" or "signal off" (Zhuo et al., 2018). In order to achieve a signal-off state, commonly used strategies included: (1) directly introducing a quencher, such as ferrocene (Zhou et al., 2017) or dopamine (Gu et al., 2019) into the ECL system; (2) *in situ* generating a quencher through enzymatic reaction (Zhao et al., 2015); (3) applying ECL resonance energy transfer (ECL-RET) (Fu et al., 2019); (4) suppressing the ECL emission through the steric hindrance of the deposition or biological identification reaction (Zhu et al., 2017); (5) utilizing nucleic acid-based cutting strategy (Chen et al., 2015). Among above strategies, the introduction of ferrocene and dopamine as ECL quencher commonly involved tedious labeling and purification procedures. The ECL-RET was a distance-dependent process, and it was limited by the choice of RET donor-acceptor pair and the distance between the donor and acceptor (Fu et al., 2019). For the strategy based on the steric hindrance, its sensitivity could not meet the requirement of highly sensitive analysis. For the nucleic acid-based cutting strategy, the shearing efficiency would be greatly restricted by the shearing conditions, such as temperature, time, and complicated pre-designed process. *In suit* generating quencher through enzymatic reaction not only addressed the shortcomings from aforementioned strategies, but also had a simple operation and a high sensitivity, thus it was a superior choice in ECL signal switching modes.

Organophosphorus (OPs) pesticides, as a typical class of pesticides, had been widely applied for crops protection to eliminate pest. However, the residues of OPs could pollute extremely the environment and have an irreversible impact on certain organs of the human body, such as nervous and respiratory system (Stocka et al., 2011). Hence, it is very valuable to detect OPs simply and sensitively. Among various determination methods for OPs, including gas-liquid chromatography (Fenoll et al., 2005; Lechtenfeld et al., 2011), electrochemistry (Liu et al., 2017), whole-cell biosensing (Khatun et al., 2018), fluorescence (Liao et al., 2013), and ECL (Wang et al., 2016), the ECL enzyme-based biosensing was a better alternative due to the simple operation, and high selectivity and sensitivity (Huang et al., 2019). Gong's group firstly constructed an ECL enzyme biosensor based on CdTe QDs as signal probe for the quantitative analysis of OPs (Liang et al., 2014). Yang's group reported an ECL enzyme biosensor for examining OPs with the luminol as luminophore (Miao et al., 2016). Our group developed a novel ECL ratiometric enzyme biosensor for OPs assay with PFO dots as anodic signal probe and graphene oxide-CdTe quantum dots as cathodic signal probe (Chen et al., 2017). Nevertheless, these reported ECL enzyme-based strategies for OPs detection not only involved the application of coreactants, and also achieved an ECL signal-off state by consuming coreactants such as dissolved O_2 or H_2O_2. Obviously, the stability or repeatability problems caused by the application of exogenous coreactants and the uncertainty of dissolved O_2 concentration could not be ignored. Therefore, it is highly significant to develop an ECL enzyme-based biosensor for OPs detection, which not only excluded exogenous species or dissolved O_2 as coreactant, but also *in situ* generated a quencher of ECL luminophore.

Fortunately, it was found that PFBT PNPs, as another polyfluorene nanoparticle, performed a high ECL emission efficiency without any external coreactants and dissolved O_2. Most importantly, H_2O_2 could efficiently quench the ECL of PFBT PNPs. Based on above facts, this work made use of PFBT PNPs to construct a coreactant-free ECL enzyme-based biosensor for the determination of OPs. Firstly, PFBT PNPs were prepared and served as a matrix for immobilizing acetylcholinesterase (AChE) and choline oxidase (ChOx). Then, the AChE-ChOx catalyzed the substrate acetylthiocholine (ATCl) to produce H_2O_2, resulting in a

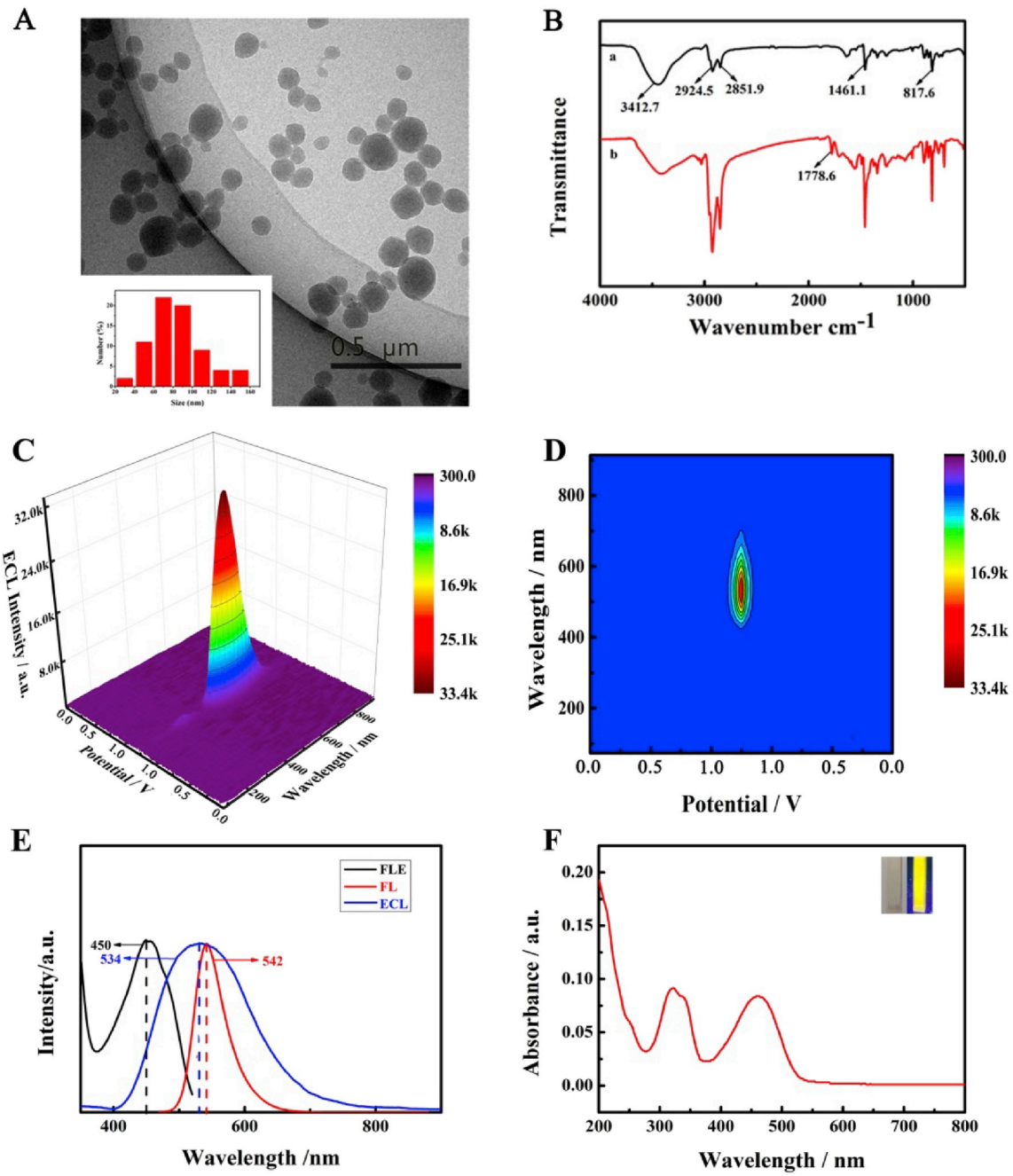

Fig. 1. (A) TEM image of PFBT PNPs (inset: size distribution); (B) FT-IR spectra of PFBT (curve a) and PFBT PNPs (curve b); (C) three-dimensional surface image and (D) heat map image of PFBT PNPs in PBS (pH 7.4) containing 20 mM TEA solution, scan potential: 0–1.25 V; (E) FL spectra (FL), FL excitation spectra (FLE) and maximum ECL emission spectra (with a potential of 1.25 V) of PFBT PNPs; (F) The UV–vis absorption spectra of PFBT PNPs (inset: the color of PFBT PNPs under visible light (left) and 356 nm UV lamp (right)). (For interpretation of the references to color in this figure legend, the reader is referred to the Web version of this article.)

signal-off state due to the quenching effect of H_2O_2 on ECL of PFBT PNPs. In the presence of OPs, OPs inhibited the enzyme active of AChE to make the quantity of product H_2O_2 declined, resulting in the recovery of ECL, thus achieving a highly sensitive detection of OPs. The wonderful combination of PFBT PNPs with excellent ECL luminous efficiency and H_2O_2 with an efficient quenching effect on the ECL of PFBT PNPs blazed a promising trail for constructing a coreactant-free ECL biosensor, especially, in the areas of enzyme-based biosensor.

2. Experimental sections

2.1. The synthesis of PFBT PNPs

PFBT PNPs were synthesized according to the literature with minor modification (Wu and Chui, 2013). Firstly, 4 mg of PFBT and 0.8 mg of PSMA were dissolved in THF with a vigorous sonication for more than 5 h to obtain 1 $mg{\cdot}mL^{-1}$ solution, respectively. Then, two solutions were sufficiently mixed and quickly injected into 10 mL of ultrapure water. Subsequently, the mixture solution was continuously sonicated until the dissolvent THF was completely evaporated under air atmosphere. Finally, a small fraction of aggregates was eradicated by filtration

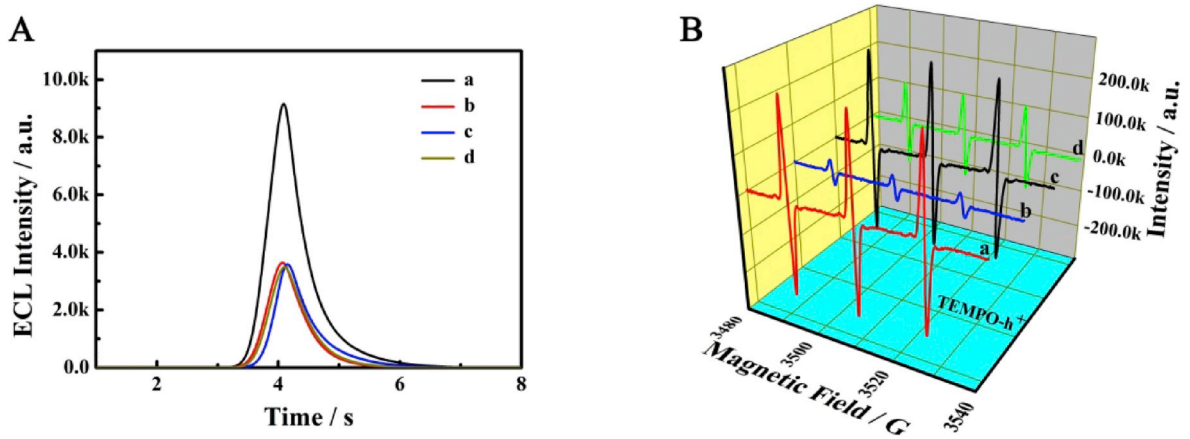

Fig. 2. (A) ECL response of PFBT PNPs/GCE in 0.10 M PBS (pH 7.4) without H_2O_2 (curve a), with 0.10 μM H_2O_2 (curve b), with 0.10 μM H_2O_2 + L-cys (curve c), and with 0.10 μM H_2O_2 + SOD (curve d), respectively; (B) EPR spectra of radical adducts trapped by TEMPO (h^+) in PFBT PNPs dispersion under dark (curve a) and light irradiation (curve b); EPR spectra of PFBT PNPs + H_2O_2 system under dark (curve c) and light irradiation (curve d).

through a 440 nm membrane filter. The synthesis of PFBT PNPs is depicted in Scheme 1A.

2.2. Fabrication of biosensor

After polished with alumina (0.3 and 0.05 μm), the glass carbon electrode (GCE) with the diameter of 4.0 mm was alternatively washed by ultrapure water and ethanol, and naturally dried in air. Next, PFBT PNPs dispersion (7 μL) was dropped on the surface of GCE. After dried at room temperature, the electrode was incubated with 10 μL of the EDC/NHS (4:1) at room temperature for 1 h to activate carboxyl groups of PFBT PNPs. Finally, the AChE-ChOx biocomposite solution (10 μL) was incubated onto the surface of electrode for 8 h at 4 °C to obtain the biosensor (AChE-ChOx/PFBT PNPs/GCE), which was deposited at 4 °C for following experiment. The fabrication of biosensor is depicted in Scheme 1B.

2.3. ECL measurement

After incubated with different concentration of OPs for 20 min at 4 °C, the biosensor was performed the ECL detection in 3.0 mL of PBS (0.10 M, pH 7.4) containing 0.27 mM ATCl. The ECL signals were recorded with modified GCE as working electrode, platinum wire as auxiliary electrode and Ag/AgCl (saturated KCl) as reference electrode. The scanning potential range of 0 V–1.25 V and the voltage of 800 V for photomultiplier tube (PMT) were set.

2.4. Sample pretreatment

Three vegetables (lettuce, cabbage and pakchoi) were washed using ultrapture water and ethanol, respectively. Then, above samples (15 g) were grinded into vegetable juice and subsequently added into 12 mL of PBS and 3 mL of ethanol in turn. Next, the resulting dispersions were rapidly centrifuged at 8000 rpm for 15 min to collect the upper sample solutions.

3. Results and discussion

3.1. Characterization of PFBT PNPs

TEM characterization was performed at PFBT PNPs. As seen from Fig. 1A, spherical particles with a diameter of 60–80 nm were observed. The size distribution histogram image is illustrated in the inset of Fig. 1A, indicating that the average size was around 70 nm.

A typical FI-IR analytical technology was further performed to reflect the composition of PFBT PNPs and the results are displayed in Fig. 1B. The absorption curve of pristine PFBT (curve a) presented the absorption peaks at 2924.5 cm^{-1} and 2851.9 cm^{-1}, which were ascribed to the antisymmetric stretching vibration of the C–H bond on the PFBT alkane chain. The peak at 817.6 cm^{-1} was from the out-of-plane deformation vibration of C–H on the alkane chain. The signal from the skeletal vibration of PFBT aromatic ring was observed at 1461 cm^{-1}. Compared with the pristine PFBT, PFBT PNPs presented a new FT-IR peak at 1778.6 cm^{-1}, which was coordinated with the –COOH. The results of FT-IR spectra indicated the successful preparation of PFBT PNPs.

Additionally, the fluorescence and ECL spectroscopy of PFBT PNPs were measured. The ECL three-dimensional surface image model and heat map image of as-synthesized PFBT PNPs were measured in 3.0 mL of PBS (pH 7.4) containing 10 μL of triethylamine (TEA) solution and the results are depicted in Fig. 1C and D, respectively. As seen, the maximum ECL wavelength was at 534 nm, which was closed to the fluorescence maximum emission wavelength locating at 542 nm (Fig. 1E), speculating that the ECL emission might be resemblance with that of photoluminescence mechanism. As seen from Fig. 1E, the fluorescence maximum excitation wavelength of PFBT PNPs was at 450 nm.

The UV–vis absorption spectrum of PFBT PNPs in aqueous solution is shown in Fig. 1F. As seen, the PFBT PNPs showed a broad absorption band in the range of 300 nm–600 nm, which was ascribed to the collapse and bending of the polymer chain, leading to a lower degree of conjugation (Wu and Chui, 2013). Two characteristic absorption peaks of PFBT PNPs were situated at 322 nm and 459 nm, respectively. The inset of Fig. 1F shows the color of PFBT PNPs under visible light radiation (left) and 356 nm UV light radiation (right), respectively. As seen, a yellower color was observed under UV light radiation.

3.2. ECL behavior of PFBT PNPs and quenching effect of H_2O_2

In order to explore the possible ECL mechanism of PFBT PNPs, the effect of dissolved O_2 was firstly investigated by testing the ECL response of PFBT PNPs modified electrode (PFBT PNPs/GCE) in 0.10 M PBS (pH 7.4) solution with air-saturated atmosphere (Fig. S1A, curve a) and N_2 atmosphere (Fig. S1A, curve b), respectively. As seen, the ECL signal intensity was almost the same in both cases, which was about 9866 a.u., indicating that dissolved oxygen was not involved in the ECL reaction, namely, dissolved O_2 didn't serve as the coreactant of PFBT PNPs.

Secondly, in order to investigate the effect of testing medium, ECL response of PFBT PNPs/GCE was tested in acetonitrile (MeCN) solution containing tetrabutylammonium hexafluorophosphate ($TBAPF_6$) as supporting electrolyte. As seen, an obviously lower ECL signal intensity was observed in MeCN solution (Fig. S1A, curve c) as compared to that

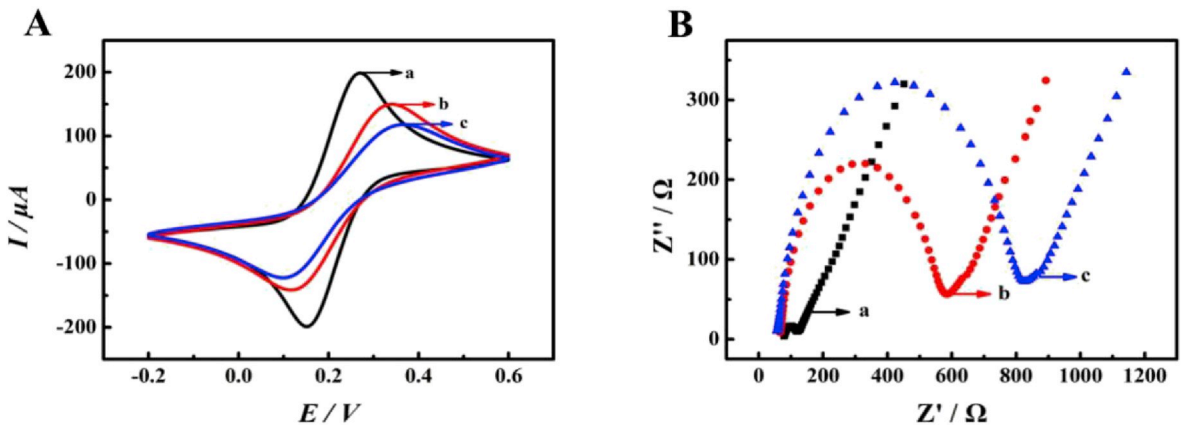

Fig. 3. (A) CV responses of (a) GCE, (b) PFBT PNPs/GCE and (c) AChE-ChOx/PFBT PNPs/GCE in 0.10 M PBS (pH 7.4) containing 5.0 mM $K_3[Fe(CN)_6]/K_4[Fe(CN)_6]$ (1:1) solution at scanning potential of −0.2–0.6 V and scanning rate of 100 mV·s^{-1}. (B) Corresponding EIS plots at a potential of 0.22 V, amplitude of 5 mV and frequency of 10^{-1}–10^5 Hz.

in PBS (pH 7.4) solution with air-saturated atmosphere (Fig. S1A, curve a), indicating that the aqueous solution was a non-negligible element.

Thirdly, the effect of the reactive oxygen species family (such as hydroxyl radicals and superoxide radicals) was investigated. L-cysteine (L-cys) and superoxide dismutase (SOD) acted as the scavengers for typical hydroxyl radicals ($OH^{\bullet}$) and superoxide radicals ($O^{2\bullet-}$), respectively (Mezyk, 1996; Zhang et al., 2005). As shown in Fig. S1B, no obvious ECL signal change was observed when PFBT PNPs/GCE was monitored in the L-cys + PBS (curve b) or SOD + PBS systems (curve c), as compared to the case without L-cys and SOD (curve a), illustrating that $OH^{\bullet}$ and $O^{2\bullet-}$ were not involved in the ECL reaction of PFBT PNPs.

Excluding the role of the reactive oxygen species family ($OH^{\bullet}$ and $O^{2\bullet-}$) in the ECL reaction of PFBT PNPs, it was speculated that the trace amount of OH^- in PBS solution might react with luminophore PFBT PNPs during the scan anodic potential. Therefore, it was also explored whether the pH of PBS solution exerted an influence during the ECL reaction of PFBT PNPs. As shown in Fig. S1C, when the pH of PBS solution was raised from 1 to 11, the ECL signal of PFBT PNPs was also boosted, suggesting that OH^- was indeed related to the ECL emission of PFBT PNPs. The possible ECL mechanisms are described in Scheme 1C. Briefly, the PFBT PNPs were firstly oxidized to yield the cation radical PFBT $PNPs^{\cdot+}$ under anodic potential scan. Then, PFBT $PNPs^{\cdot+}$ reacted with OH^- to produce free radical PFBT PNPs through losing protons. Finally, the excited stated PFBT PNPs* was produced when PFBT PNPs met with PFBT $PNPs^{\cdot+}$, thus emerging the ECL emission. In fact, similar ECL reactions between OH^- and luminophore have been reported (Zheng et al., 2009; Feng et al., 2016).

In addition, the obstruction of H_2O_2 on the ECL emission of PFBT PNPs was further explored through ECL and electron paramagnetic resonance (EPR) assay. As shown in Fig. 2A, in 0.10 M PBS testing solution, an ECL peak with a high intensity was observed at PFBT PNPs/GCE (curve a). When 0.10 μM H_2O_2 was introduced into the testing solution, a weak ECL intensity was noted (curve b). In order to explore whether the quenching effect was caused by more $OH^{\bullet}$ and $O^{2\bullet-}$ derived from H_2O_2, the ECL response of PFBT PNPs/GCE was monitored in 0.10 M PBS containing both H_2O_2 and L-cys (curve c) or both H_2O_2 and SOD (curve d). As observed, the quenching effect of H_2O_2 was almost unchanged with or without L-cys and SOD, showing that $OH^{\bullet}$ and $O^{2\bullet-}$ derived from H_2O_2 might not be considered as the quencher to attenuate ECL signal. The EPR measurement was further utilized to explore the hole (h^+) of PFBT PNPs. As shown in Fig. 2B, strong peaks from the typical TEMPO radical triplet were observed when PFBT PNPs were placed in the dark environment without (curve a) and with (curve c) H_2O_2. Moreover, the signal strength was almost identical in both cases. Under the irradiation, PFBT PNPs presented a very low signal strength in the TEMPO radical EPR spectra (curve b), which was due to the generation of photogenerated h^+ of PFBT PNPs. With the addition of H_2O_2 in PFBT PNPs dispersion, the signal intensity of TEMPO radical EPR spectra was obviously increased (curve d). The possible reasons may be as follows. Under the irradiation, the photogenerated h^+ could directly oxide the H_2O_2 (Du et al., 2019), resulting in a decrease in the amount of h^+, thereby blocking the ECL emission of PFBT PNPs. The quenching effect

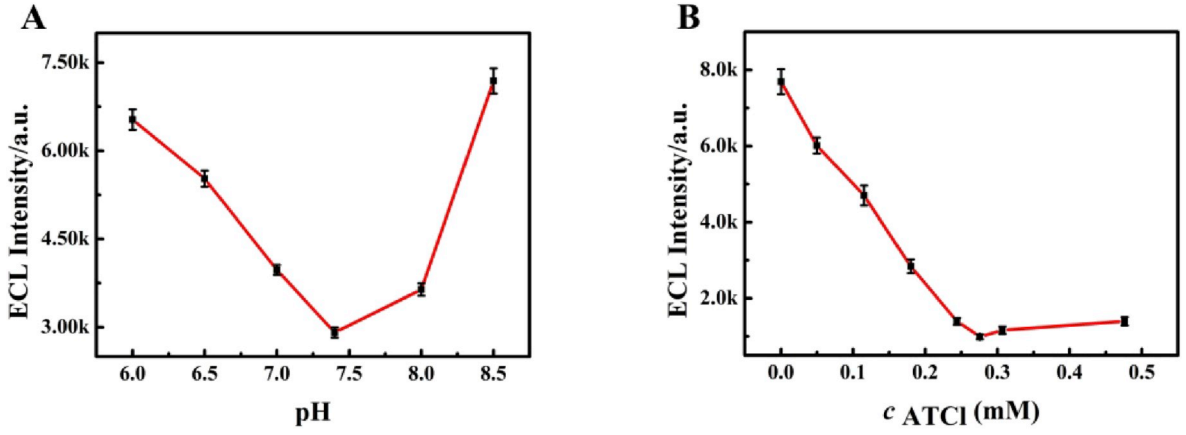

Fig. 4. (A) The effect of pH on the ECL at AChE-ChOx/PFBT PNPs/GCE in 0.10 M PBS containing 0.27 mM ATCl; (B) The effect of ATCl concentration on the ECL of AChE-ChOx/PFBT PNPs/GCE. Scanning potential range: 0–1.25 V, scanning rate: 300 mV·s^{-1}.

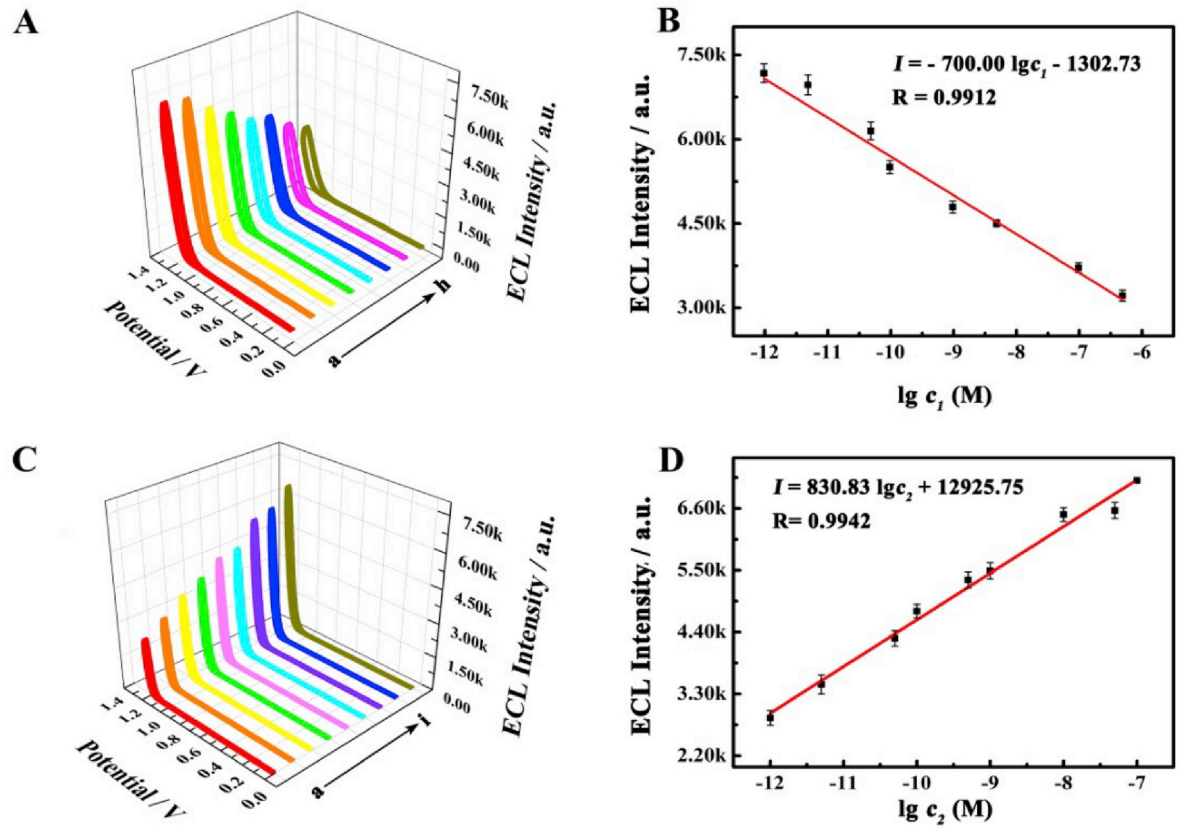

Fig. 5. (A) ECL response of PFBT PNPs/GCE towards H_2O_2, from (a) to (h): 9.68×10^{-13}, 4.84×10^{-12}, 4.84×10^{-11}, 9.68×10^{-11}, 9.68×10^{-10}, 4.84×10^{-9}, 9.68×10^{-8}, and 4.84×10^{-7} M. (C) ECL response of AChE-ChOx/PFBT PNPs/GCE towards OPs, from (a) to (i): 1.0×10^{-12}, 5.0×10^{-12}, 5.0×10^{-11}, 1.0×10^{-10}, 5.0×10^{-10}, 1.0×10^{-9}, 1.0×10^{-8}, 5.0×10^{-8}, 1.0×10^{-7} M. (B) and (D): the calibration curve for H_2O_2 and OPs detection, respectively. Scanning potential range: 0–1.25 V, scanning rate: 300 $mV \cdot s^{-1}$.

of H_2O_2 on the ECL emission of PFBT PNPs and the response mechanisms of the biosensor towards OPs are illustrated in Scheme 1B.

3.3. The characterization of the assembly process of biosensor

The different assemble steps of as-prepared biosensor were characterized through cyclic voltammetry (CV) and electrochemical impedance spectroscopy (EIS), and the results are shown in Fig. 3A. Compared with the bare GCE (curve a), the PFBT PNPs modified electrode (curve b) presented a declining redox peak current due to the poor conductivity of PFBT PNPs. When the AChE-ChOx biocomposites were incubated onto the surface of electrode *via* the pathway of cross-linking, a weaker peak current was observed due to the obstruction of non-conductive biomacromolecule (curve c). At the same time, the assembly procedure of as-prepared biosensor was monitored using EIS technique and the results are displayed in Fig. 3B. The same results between EIS characterization and CV characterization were obtained, indicating that the proposed biosensor was successfully constructed as expectedly.

Table 1
Comparison of different sensor for the determination of OPs.

Electrode material	Detection method	Linear range(M)	Detection limit(M)	Reference
P3HT/TiO2/ ITO	PEC	2.0×10^{-7}- 1.6×10^{-6}	1.0×10^{-8}	Li et al. (2011)
Au-PtNPs/3-APTES/GCE	amperometry	1.5×10^{-7}- 2.0×10^{-7}	–	Upadhyay et al. (2009)
Au-PPy-rGO/ GCE	amperometry	1.0×10^{-9}- 5.0×10^{-6}	5.0×10^{-11}	Yang et al. (2014)
Pt–Au/ MWCNT/ GCE	ECL	5.0×10^{-8}- 5.0×10^{-7}	3.0×10^{-8}	Miao et al. (2016)
PFBT PNPs/ GCE	ECL	1.0×10^{-12}- 1.0×10^{-7}	1.5×10^{-13}	This work

3.4. Optimization of experimental conditions

The parameters including pH of PBS solution and the substrate concentration of ATCl were optimized to obtain the best ECL properties of as-proposed biosensor. As the activity of enzyme and ECL intensity of PFBT PNPs depended on the pH of PBS solution, pH of PBS solution was firstly optimized at a constant substrate concentration of 0.27 mM. As seen in Fig. 4A, when the pH of PBS solution increased from 6.0 to 7.4, the ECL intensity gradually decreased, which was attributed to an increase in the amount of H_2O_2 *in situ* generated in the enzymatic reaction. The ECL signal reached the minimum value at 7.4, indicating the maximum amount of produced H_2O_2. As the pH exceeded 7.4, the ECL signal increased with raising pH, which may be due to the inhibition of enzyme activity of the AChE and ChOx under high pH condition, resulting in a decreased amount of produced H_2O_2. Thus, pH 7.4 was used in the following experiment.

The ATCl could be utilized for *in situ* generating quencher H_2O_2, thus the concentration of ATCl was considered as another key factor to obtain the optimitized ECL performance. As seen in Fig. 4B, the ECL signal constantly decreased with increasing ATCl concentration from 0.00 mM to 0.27 mM and reached the minimum value at 0.27 mM, suggesting that the activity center of enzymes had been completely occupied by substrate ATCl in the case of 0.27 mM (Chen et al., 2017). Thus, 0.27 mM ATCl was chosen for following experiment to obtain a low ECL background signal.

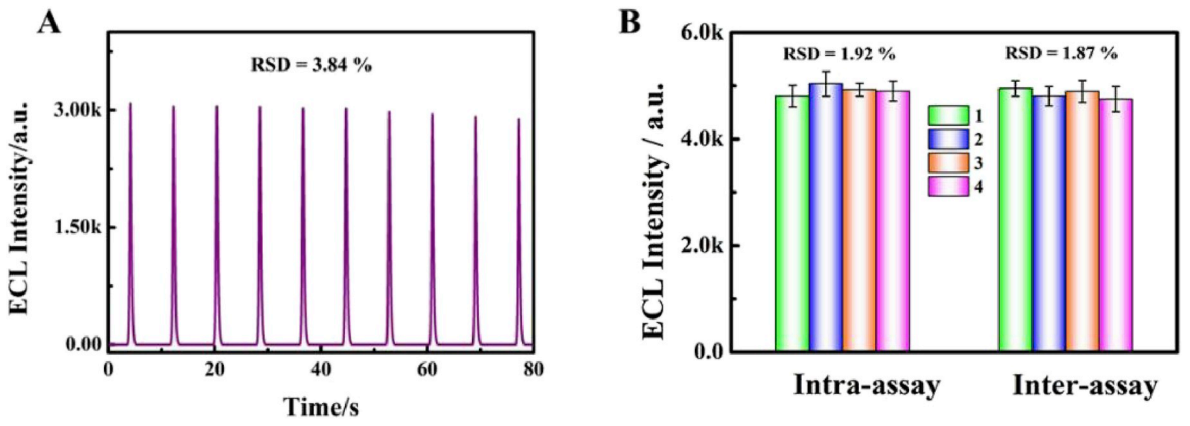

Fig. 6. (A) The ECL signal of as-prepased biosensor under continuous cyclic potential scan for 10 cycles in the presence of 5.0×10^{-12} M OPs; (B) the ECL response of intra- and inter-assay of the AChE-ChOx/PFBT PNPs/GCE towards 5.0×10^{-11} M OPs.

3.5. ECL response for OPs

In order to confirm the application of PFBT PNPs in biosensing system, we firstly constructed a H_2O_2 sensor *via* directly applying PFBT PNPs modified GCE and the result is shown in Fig. 5A. The ECL signal of PFBT PNPs was reduced with raising H_2O_2 concentration. The linear variation was observed between the signal strength and the logarithm of H_2O_2 concentration (Fig. 5B). The linear range for H_2O_2 was from 9.9×10^{-13} to 4.8×10^{-7} M, and the linear equation was expressed as $I = -700.003\ lgc_1 - 1302.734$ with the detection limit of 3.3×10^{-13} M. The highly sensitive ECL response of PFBT PNPs/GCE towards H_2O_2 further confirmed the quenching effect of H_2O_2 on the ECL emission of PFBT PNPs.

When AChE and ChOx were modified onto the PFBT PNPs/GCE for the quantitative analysis of OPs, due to the inhibition of target OPs on the activity of AChE, the H_2O_2 produced by enzymatic reaction was reduced, resulting in an amplified ECL signal with increasing OPs concentration (Fig. 5C). A linear variation between the ECL intensity and the logarithm of the OPs concentration was obtained in the concentration range of 1.0×10^{-12}–1.0×10^{-7} M (Fig. 5D), and the linear equation was $I = 830.83\ lgc_2 + 12925.75$. The correlation coefficient and detection limit were 0.9942 and 1.5×10^{-13} M (S/N = 3), respectively. Compared to previous strategies for OPs detection, the constructed biosensor exhibited a more excellent sensitivity and a wider linear range owing to the high ECL efficiency of PFBT PNPs and efficient quenching effect of H_2O_2, and the comparison is shown in Table 1.

3.6. The stability and reproducibility of biosensor

In the case of the biosensor incubated with 5.0×10^{-12} M OPs, the stability of the biosensor was explored by detecting the ECL response of the biosensor in 0.10 M PBS in the case of continuous cyclic scan for 10 circles. Fig. 6A clearly shows an almost identical ECL signal and the RSD was around 3.84%, indicating a good stability of the biosensor. Additionally, the reproducibility was further estimated *via* the intra- and inter-assays. As seen in Fig. 6B, the ECL response towards 5.0×10^{-11} M OPs at four biosensors from the same or different batch expressed a negligible difference in intra- and inter-assays. And the RSD was all below 3%. It suggested that the constructed biosensors had an acceptable reproducibility.

3.7. Real analysis for different vegetable

Lettuce, cabbage and pakchoi, which were obtained from local supermarket, were selected as the practical samples to study the availability of as-proposed biosensor. Lettuce, cabbage and pakchoi were carried out a preliminary treatment (Chen et al., 2017) and stored at 4 °C. Recovery experiments were performed using above three sample solutions by standard addition method. The results are shown in Table S1. No residual OPs was detected in lettuce, cabbage and pakchoi sample solution, and the recovery rates were 93.0%–98.8%, 93.0%–103%, and 97.5%–101%, respectively, intimating that the coreactant-free ECL enzymatic biosensor has a potential availability for rapid and sensitive detection of OPs in real bioanalysis.

4. Conclusion

PFBT PNPs exhibited a high ECL luminescent efficiency in the absence of any external coreactants. Furthermore, the quenching effect of H_2O_2 on the ECL emission of PFBT PNPs was found. A coreactant-free ECL enzyme biosensor for OPs detection was constructed with the integration of PFBT PNPs and H_2O_2. Such an ECL strategy avoided the drawbacks of the application of exogenous species or dissolved O_2 as coreactant, thus providing a promising ECL platform for bioanalysis.

Supporting information

Supporting information includes the following contents: Reagents and Materials; Apparatus; The ECL behavior of PFBT PNPs (Fig. S1); **The recovery rates of OPs in different vegetable samples** (Table S1); **The details of detection limit**.

Declaration of competing interest

The authors declare that they have no known competing financial interests or personal relationships that could have appeared to influence the work reported in this paper.

Acknowledgments

This work was supported by National Natural Science Foundation of China (21775122, 21775124, 51473136, 21575116), and Natural Science Foundation of Chongqing City (cstc2018icyjAX0693), China.

Appendix A. Supplementary data

Supplementary data to this article can be found online at https://doi.org/10.1016/j.bios.2019.111898.

References

Chen, Y., Xiang, Y., Yuan, R., Chai, Y.Q., 2015. Nanoscale 7, 981–986.
Chen, H.M., Lu, Q.Y., Liao, J.Y., Yuan, R., Chen, S.H., 2016. Chem. Commun. 52, 7276–7279.
Chen, H.M., Zhang, H., Yuan, R., Chen, S.H., 2017. Anal. Chem. 89, 2823–2829.

Chinnadayyala, S.R., Park, J., Le, H.T.N., Santhosh, M., Kadam, A.N., Cho, S.B., 2019. Biosens. Bioelectron. 126, 68–81.
Du, M.X., Du, Y., Feng, Y.B., Li, Z.F., Wang, J.Y., Jiang, N., Liu, Y., 2019. Cellulose 26, 5543–5557.
Feng, Y.Q., Dai, C.H., Lei, J.P., Ju, H.X., Cheng, Y.X., 2016. Anal. Chem. 88, 845–850.
Feng, Y.Q., Wang, N.N., Ju, H.X., 2018. Anal. Chem. 90, 1202–1208.
Fenoll, J., Hellin, P., Marin, C., Martinez, C.M., Flores, P., 2005. J. Agric. Food Chem. 53, 7661–7666.
Fu, X.L., Hou, F., Liu, F.R., Ren, S.W., Cao, J.T., Liu, Y.M., 2019. Biosens. Bioelectron. 129, 72–78.
Gu, Y., Wang, J.P., Shi, H.P., Pan, M.F., Liu, B., Fang, G.Z., Wang, S., 2019. Biosens. Bioelectron. 128, 129–136.
Huang, Y.Y., Ren, J.S., Qu, X.G., 2019. Chem. Rev. 119, 4357–4412.
Jiang, M.J., Li, S.K., Zhong, X., Liang, W.B., Chai, Y.Q., Zhuo, Y., Yuan, R., 2019. Anal. Chem. 91, 3710–3716.
Khatun, M.A., Hoque, M.A., Zhang, Y., Lu, T., Cui, L., Zhou, N.Y., Feng, Y., 2018. Anal. Chem. 90, 10577–10584.
Kitte, S.A., Gao, W.Y., Zhoudov, Y.T., Qi, L.M., Nsabimana, A., Liu, Z.Y., Xu, G.B., 2017. Anal. Chem. 89, 9864–9869.
Lechtenfeld, O.J., Koch, B.P., Geibert, W., Ludwichowski, K.U., Kattner, G., 2011. Anal. Chem. 83, 8968–8974.
Li, H.B., Li, J., Xu, Q., Hu, X.Y., 2011. Anal. Chem. 83, 9681–9686.
Liang, H., Song, D.D., Gong, J.M., 2014. Biosens. Bioelectron. 53, 363–369.
Liao, S.Z., Han, W.T., Ding, H.Z., Xie, D.X., Tan, H., Yang, S.Y., Wu, Z.Y., Shen, G.L., Yu, R.Q., 2013. Anal. Chem. 85, 4968–4973.
Liu, X.J., Song, M.M., Hou, T., Li, F., 2017. ACS Sens. 2, 562–568.
Luo, J.H., Cheng, D., Li, P.X., Yao, Y., Chen, S.H., Yuan, R., Xu, W.J., 2018. Chem. Commun. 54, 2777–2780.
Mezyk, S.P., 1996. J. Phys. Chem. 100, 8295–8301.
Miao, S.S., Wu, M.S., Ma, L.Y., He, X.J., Yang, H., 2016. Talanta 158, 142–151.
Muzyka, K., Saqib, M., Liu, Z.Y., Zhang, W., Xu, G.B., 2017. Biosens. Bioelectron. 92, 241–258.
Qin, X.L., Gu, C.Y., Wang, M.H., Dong, Y.F., Nie, X., Li, M.X., Zhu, Z.W., Yang, D., Shao, Y.H., 2018. Anal. Chem. 90, 2826–2832.
Sha, H.F., Zhang, Y., Wang, Y.F., Ke, H., Xiong, X., Jia, N.Q., 2019. Biosens. Bioelectron. 124, 59–65.
Stewart, A.J., Brown, K., Dennany, L., 2018. Anal. Chem. 90, 12944–12950.
Stocka, J., Tankiewicz, M., Biziuk, M., Namiesnik, J., 2011. Int. J. Mol. Sci. 12, 7785–7805.
Upadhyay, S., Rao, G.R., Sharma, M.K., Bhattacharya, B.K., Rao, V.K., Vijayaraghavan, R., 2009. Biosens. Bioelectron. 25, 832–838.
Wang, Y., Lu, J., Tang, L.H., Chang, H.X., Li, J.H., 2009. Anal. Chem. 81, 9710–9715.
Wang, H.J., Yuan, R., Chai, Y.Q., Niu, H., Cao, Y.L., Liu, H.J., 2012. Biosens. Bioelectron. 37, 6–10.
Wang, B.X., Wang, H.J., Zhong, X., Chai, Y.Q., Chen, S.H., Yuan, R., 2016. Chem. Commun. 52, 5049–5052.
Wang, S.S., Zhao, Y.Y., Wang, M.M., Li, H.J., Saqib, M., Ge, C.H., Zhang, X.D., Jin, Y.D., 2019. Anal. Chem. 91, 3048–3054.
Wu, C.F., Chui, D.T., 2013. Angew. Chem. Int. Ed. 52, 3086–3109.
Wu, C.F., Bull, B., Szymanski, C., Christensen, K., Mcneill, J., 2008. ACS Nano 2 (11), 2415–2423.
Yang, Y.Q., Asiri, A.M., Du, D., Lin, Y.H., 2014. Analyst 139, 3055–3060.
Zhang, L., Tang, B., Ding, Y., 2005. J. Agric. Food Chem. 53, 549–553.
Zhao, M., Liao, N., Zhuo, Y., Chai, Y.Q., Wang, J.P., Yuan, R., 2015. Anal. Chem. 87, 7602–7609.
Zheng, L.Y., Chi, Y.W., Shu, Q.Q., Dong, Y.Q., Zhang, L., Chen, G.N., 2009. J. Phys. Chem. C 113, 20316–20321.
Zhou, Y., Wang, H.J., Zhuo, Y., Chai, Y.Q., Yuan, R., 2017. Anal. Chem. 89, 3732–3738.
Zhou, Y., Wang, H.J., Lei, Y.M., Zhang, P., Liu, J.L., Chai, Y.Q., Yuan, R., 2018. Analyst 143, 3230–3248.
Zhu, S., Lin, X., Ran, P.Y., Xia, Q., Yang, C.C., Ma, J., Fu, Y.Z., 2017. Biosens. Bioelectron. 91, 436–440.
Zhuo, Y., Wang, H.J., Zhang, H., Chai, Y.Q., Yuan, R., 2018. Anal. Chem. 90, 3543–3549.